PROCEEDINGS OF SCIENCE

Maser observations - from the kinematics to the physics of evolved star winds.

A. M. S Richards[*ab], **K. A. Assaf**[a], **I. Bains**[c], **A. Bartkiewicz**[d], **P. J. Diamond**[a], **M. Elitzur**[e], **S. Etoka**[a], **M. D. Gray**[a], **E. A. Humphreys**[f], **K. Murakawa**[g], **M. Szymczak**[d], **H. J. van Langevelde**[h], **J. A. Yates**[i]

[a] *JBCA, Department of Physics and Astronomy, University of Manchester, M13 9PL, UK.*
[b] *UK ALMA Regional Centre,, Department of Physics and Astronomy, University of Manchester, M13 9PL, UK.*
[c] *Swinburne University of Technology, Victoria, Australia*
[d] *Toruń Centre for Astronomy, Nicolaus Copernicus University, Poland*
[e] *University of Kentucky, Department of Physics and Astronomy, USA*
[f] *ESO, D-85748 Garching-bei-München, Germany*
[g] *MPIfR, 53121 Bonn, Germany*
[h] *Leiden University & JIVE, PO Box 2, NL-7990 AA Dwingeloo, NL*
[i] *Department of Physics and Astronomy, UCL, London WC1E 6BT, UK*
E-mail: amsr@jb.man.ac.uk

We have monitored cm-wave masers in circumstellar envelopes using MERLIN and VLBI. These images resolve the AU-scale structure and kinematics of the winds and reveal how cloud sizes and incipient asymmetries appear to depend on the stellar masses and magnetic fields. The water maser monitoring data also allows us to differentiate between models for matter-bounded and amplification-bounded masers. We find that the clouds in most sources are on average spherical, but flattened emission regions are present in some Miras which also show other evidence for the presence of shocks. The water maser clouds are found to be denser than their surroundings, but the exponential nature of maser amplification has hitherto made it very hard to reconstruct precise physical conditions. We look ahead to the opportunities to remedy this problem provided by EVN developments, the EVLA, e-MERLIN and in particular Early Science with ALMA.

10th European VLBI Network Symposium and EVN Users Meeting: VLBI and the new generation of radio arrays
September 20-24, 2010
Manchester, UK

[*] Speaker.

PoS(10th EVN Symposium)005

1. Introduction

The bulk of dust and light elements are returned to the ISM by post-main-sequence stars. Asymptotic Giant Branch (AGB) stars with progenitor masses ≤ 8 $M_\odot$ have mass loss rates $10^{-7} - 10^{-5}$ $M_\odot$ yr^{-1}, in the form of cool, molecular winds. Higher-mass Red Supergiants (RSG) can lose mass at ten times this rate or even more and were particularly significant in enriching the early universe. We do not fully understand the stellar mass loss mechanisms. Recent work by [15] suggests that the popular mechanism combining stellar pulsation and silicate dust is insufficient for O-rich stars, although coordinated VLTI and VLBA observations of Al_2O_3 grains and SiO masers [14] suggests that dust nucleation is associated with driving mass loss. Nor do we know why apparently solitary stars produce axisymmetric circumstellar envelopes (CSE) and nebulae.

We began high-resolution monitoring of H_2O and OH masers in CSE in 1994, using MERLIN, EVN/Global VLBI and single-dish monitoring. The combination of Doppler and proper motion velocity measurements has shown that the mass loss is predominantly radial ([12], [8]). The H_2O masers emanate from discrete clouds which are 30 to $>$100 times denser than their surroundings ([11], [1]), which support OH mainline masers towards the outer parts of the H_2O maser shell.

This contribution focuses on one aspect of our results, the first direct observational test of models of H_2O maser beaming in CSEs, described in Section 2. Masers are good kinematic tracers but it is harder to model unique combinations of temperature, density and abundances. Multiple lines provide tighter constraints in star-forming regions but in any given region of a CSE only one cm-wave transition is usually detected, apart from the pair of OH ground-state main lines (attempts to detect excited OH have failed before the post-AGB stage) and, as yet, thermal lines cannot be resolved on such small scales. We summarise how the next generation of interferometers will allow us to track the composition as well as the structure and kinematics of mass loss in Section 3.

2. Cloud structure deduced from maser beaming models

Five of the objects in our sample are at high enough Declination and were observed at multiple epochs with good enough *uv* coverage to make very accurate spatial measurements. MERLIN imaging at 22 GHz detects essentially all the maser emission detected by single dish observations, with enough sensitivity to measure the complete size of maser clouds (as demonstrated by [11]). We imaged the RSG S Per and four AGB stars, RT Vir, IK Tau, U Her and U Ori, for between 2 and 7 epochs per star. The position and size of each patch of maser emission, in each 0.1 or 0.2, km s^{-1} velocity channel, can be measured with sub-mas accuracy. The total extent of each maser clump can be estimated from the maximum separation of the masers at the extreme velocities within each series of components (Fig. 1). These clouds are typically of a similar size to the star (one or two AU in radius on the AGB), while the observed size of individual components ranges from the minimum measurable, about 0.025 AU, up to the cloud size. Fig. 1 *right* shows that the apparent component size shrinks towards the peak of the line profile of the emission from a typical S Per cloud, also seen for RT Vir and (at most epochs) IK Tau. However, Fig. 2 shows that in U Ori, the components making up many maser clouds have no obvious size dependence across the line profile or are largest near the peaks. Such behaviour is also seen in U Her.

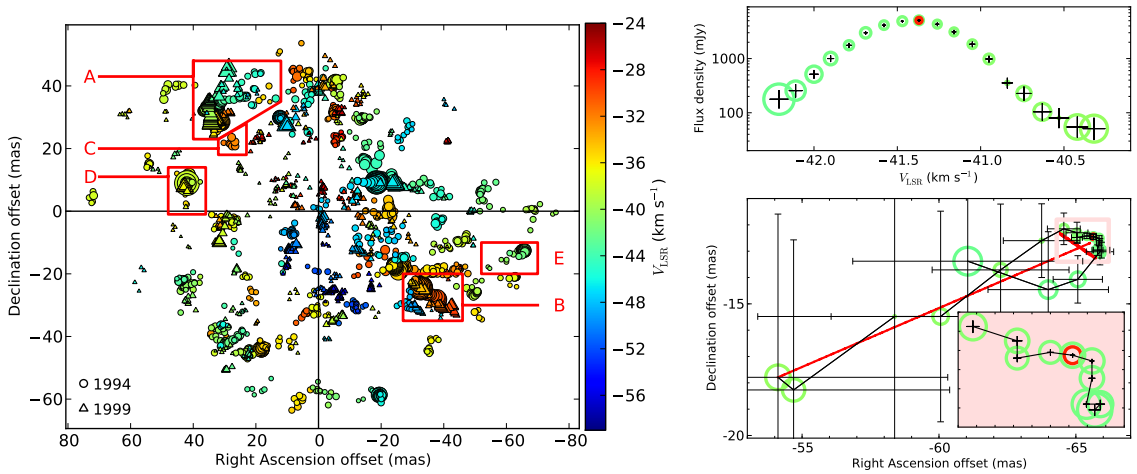

Figure 1: *left* Each symbol represents an H_2O maser component in a single channel observed towards S Per. The diameter is proportional to the square root of total intensity. *right* Maser clump E: *Top*: Clump line profile, symbol diameters proportional to s_v; the error bars show the size uncertainty σ_s. *Bottom*: Detailed map of the components comprising the clump. The symbol diameter is 10% of s_v and the error bars represent the position uncertainties. The thin black line joins the components in velocity order. The expanded-scale inset (total size 1.7×1.2 mas) shows the area in the pink box, which contains the components brighter than half maximum, with component size error bars. The brightest component is outlined in red.

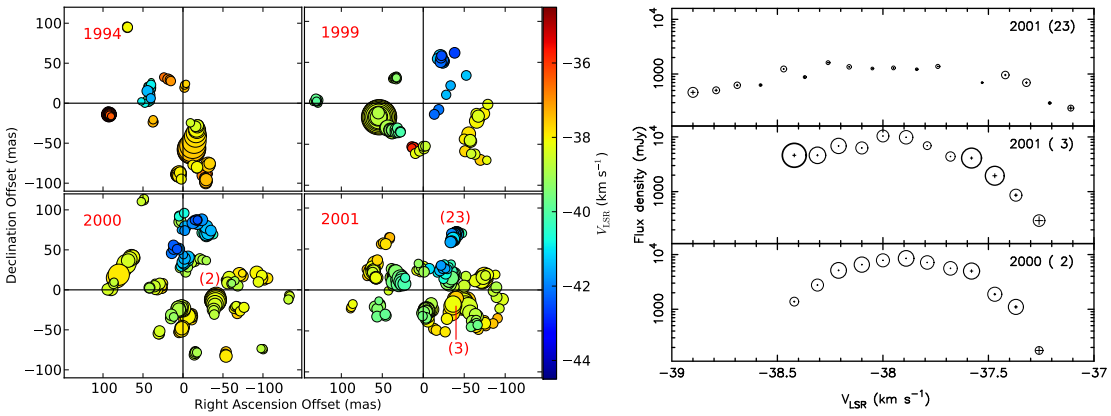

Figure 2: *left* As Fig. 1, for U Ori, at the four epochs indicated. *right* Line profiles of the labelled clumps.

Elitzur [3] derived expressions for two types of masing. 'Amplification-bounded' beaming occurs when a maser propagates through a spherical cloud; the central rays are much more strongly amplified and the observed FWHM of the maser in any given small velocity interval is much smaller than the emission region. 'Matter-bounded' beaming emanates from cylindrical or other elongated regions, seen down the long axis, where similar amplification takes place across the surface and the apparent size is reduced less or not at all. Using expressions from [4], as explained in [13] for the effect of unsaturated maser amplification by spherical clouds, $s_v \propto 1/\sqrt{\ln I_v}$, where I_v is the flux density of a maser component, angular FWHM s_v. A plot of $\log s_v$ as a function of $\log \ln I_v$ should have a slope of -0.5. Fig. 3 *left* shows gradients in the expected sense for S Per; the slope for

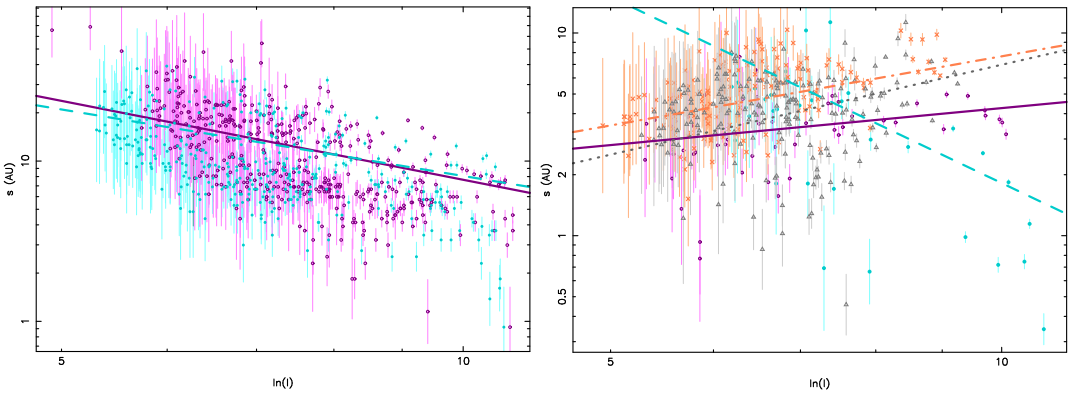

Figure 3: Maser component FWHM s_v as a function of the natural logarithm of the intensity I_v, for components where $s_v > 3\sigma_s$. The different colours show different epochs. The corresponding error-weighted least-squares fits (to all data) are shown. Results for S Per are shown on the *left* and for U Ori on the *right*.

all data is < -1 due to the steeper narrowing of the brightest components which are approaching saturation. RT Vir has an average gradient of –0.5 for 7 epochs of data and IK Tau has a negative slope for 2 out of 3 epochs. In contrast, U Ori (Fig. 3 *right*) and U Her have positive slopes at all but one epoch, with very large scatters.

Fig. 4 illustrates these types of behaviour. The inverse relationship between H_2O maser brightness and observed component size suggests that S Per, RT Vir and IK Tau exhibit amplification-bounded maser amplification by approximately spherical clouds. On the other hand, the size of U Ori and U Her maser components is often larger near the features peaks. This more varied behaviour is consistent with matter-bounded masing from clouds flattened by shocks. This allows strong amplification through the long axis of the cloud, perpendicular to the shock, whilst the shorter axes are optically thin at the IR wavelengths involved in the pump. These sources have the deepest and most regular pulsation periods, so shocks could propagate more strongly into the H_2O maser shell and flatten the clouds. Moreover, both U Ori and U Her have undergone OH maser flares likely to have originated in the inner CSE ([9]; [2]; [5]).

These relationships, between the observed size of maser emission in single channels, and the overall shape of clouds, provide a useful diagnostic for the presence of discrete clouds and/or shocked regions.

3. Tracing mass loss from photosphere to ISM

We find that the average radius of 22-GHz H_2O maser clouds is broadly proportional to the stellar radius. This suggests that the clumping scale of the stellar wind is determined by the macroscopic behaviour of the star itself, not by microscopic-scale properties of the wind (e.g. cooling associated with remote dust formation). If the clouds expand due to radial acceleration, their birth sizes extrapolated back to the stellar surface are about 0.1 $R_\star$. Their origin could be in star spots and/or convection cells. Optical/IR interferometry and the VLA have measured the diameters and gross irregularities of a number of evolved stars (e.g. [10]), but such observations lack sufficient *uv* coverage and/or resolution to resolve details. The only well-resolved star to date (apart from the Sun) is Betelgeuse, using MERLIN+VLA [7] and the *HST*.

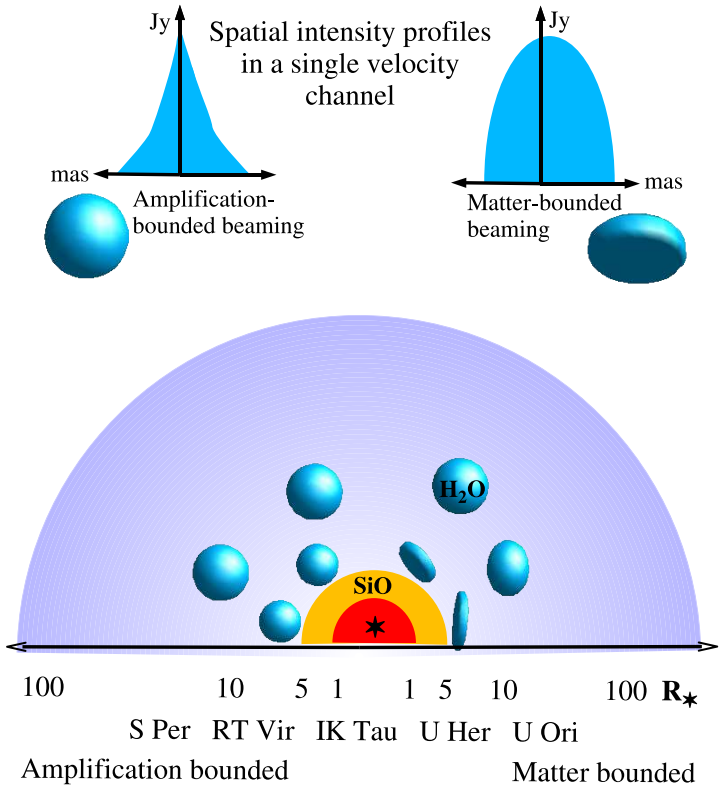

Figure 4: This cartoon shows (left to right) spherical or flattened water vapour clouds in a CSE (not to scale). The upper diagrams show the spatial profiles resulting from maser propagation through a sphere (*left*) and through a disc seen edge-on (*right*). The sources are listed in order corresponding to the degree to which they exhibit either behaviour.

A number of stars in our sample are large and bright enough to be well-resolved by e-MERLIN (plus the EVLA at higher frequencies) and eventually ALMA. The stellar radius at which the photosphere becomes optically thick is greater at longer wavelengths, so a series of observations over several months at decreasing frequencies would track disturbances propagating outwards from the star. The spectral indicies and any spatial correlation will reveal the relative importance of pulsation or convection. These observations will be correlated with VLBI SiO maser monitoring of mass leaving the star within $2-4\ R_\star$. We will also monitor the transitions between the SiO and H_2O maser zones and between H_2O and OH, using MERLIN + EVN. These observations will reveal whether the same clouds can be traced all the way from the star to the outer CSE.

3.1 Structure of OH emitting regions

We are reducing four epochs of monitoring of OH masers using the EVN (correlated at Socorro) which will show the location and kinematics of the OH mainline regions. However, VLBI alone resolves-out between 10% and $>90\%$ of the emission. This means that we cannot analyse the maser physics adequately. In future, we will use the new correlation capacities of JIVE/EVN and e-MERLIN to make well-coordinated observations in matching spectral configurations, detecting and resolving *all* the emission. This will allow us to, for example, deduce the true size and shape of

individual masing regions using the method summarise in Section 2. e-MERLIN plus EVN are also needed to determine accurately the extent and shape of outer OH maser shells. This will help to ascertain the extent and persistence of axisymmetry and also is required to supplement single-dish monitoring using the phase-lag method to measure the distances to these stars.

3.2 ALMA

ALMA presents the first opportunity to obtain highly sensitive mm- and sub-mm-wave observations at sub-arcsec resolution, with the astrometric accuracy intrinsic to interferometry. Firstly, this will allow us to probe deeper layers of the star, where convection has stronger effects than the layers accessible at cm wavelengths. Secondly, dust and thermal lines will be imaged. When complete, ALMA will be able to resolve individual dust clouds and test the association with H_2O masers. Thirdly, there is a wealth of excited state SiO, H_2O and other maser transitions in all ALMA bands, see e.g. [6]. We will establish which transitions are co-spatial, interleaved or segregated. The conditions required for the excitation of multiple masers provide much better constraints on the physical properties and abundances in emission regions. This could show, for example, whether the clouds seen in water masers are chemically distinct from their surroundings or whether they are differentiated solely by temperature, density etc.

ALMA Early Science will start in 2011 with 16 antennas (out of the eventual 66) in compact configurations giving resolutions from a few hundred mas upwards. This will be sufficient to measure the overall extent of various maser transitions and to resolve .the dust formation radius for nearby CSE. It will be easy to locate stars at mm wavelengths although we will have to wait for the longer baselines to resolve the photospheres properly.

References

[1] Bains, I. et al. 2003, MNRAS, 342, 8

[2] Chapman, J. M. & Cohen, R. J. 1985, MNRAS, 212, 375

[3] Elitzur, M., Hollenbach, D. J. & McKee, C. F. 1992, ApJ, 394, 221

[4] Elitzur, M. 1992, *Astronomical Masers*, Kluwer

[5] Etoka, S. & Le Squeren, A. M. 1997, A&A, 321, 877

[6] Humphreys, E. M. L. 2007, IAU, 242, 471

[7] Lim, J., Carilli, C. L., White, S. M., Beasley, A. J., & Marson, R. G. 1998, Nat, 392, 575

[8] Murakawa, K., Yates, J. A., Richards, A. M. S., & Cohen, R. J. 2003, MNRAS, 344, 1

[9] Pataki, L. & Kolena, J. 1974, Bull. Am. astr. Soc., 6, 340

[10] Reid, M. J., & Menten, K. M. 2007, ApJ, 671, 2068

[11] Richards, A. M. S., Yates, J. A. & Cohen, R. J. 1999, MNRAS, 306, 954

[12] Richards, A. M. S., Cohen, R. J., Bains, I., & Yates, J. A. 1999, in *IAU 191: AGB Stars*, 191, 315

[13] Richards, A. M. S., Elitzur, M., & Yates, J. A. 2010, A&A, arXiv:1010.4419

[14] Wittkowski, M., Boboltz, D. A., Ohnaka, K., Driebe, T., & Scholz, M. 2007, A&A, 470, 191

[15] Woitke, P. 2006, A&A, 460, L9